

**Contract No:**

This document was prepared in conjunction with work accomplished under Contract No. DE-AC09-08SR22470 with the U.S. Department of Energy (DOE) Office of Environmental Management (EM).

**Disclaimer:**

This work was prepared under an agreement with and funded by the U.S. Government. Neither the U. S. Government or its employees, nor any of its contractors, subcontractors or their employees, makes any express or implied:

- 1 ) warranty or assumes any legal liability for the accuracy, completeness, or for the use or results of such use of any information, product, or process disclosed; or
- 2 ) representation that such use or results of such use would not infringe privately owned rights; or
- 3) endorsement or recommendation of any specifically identified commercial product, process, or service.

Any views and opinions of authors expressed in this work do not necessarily state or reflect those of the United States Government, or its contractors, or subcontractors.

We put science to work.™



**Savannah River  
National Laboratory®**

OPERATED BY SAVANNAH RIVER NUCLEAR SOLUTIONS

A U.S. DEPARTMENT OF ENERGY NATIONAL LABORATORY • SAVANNAH RIVER SITE • AIKEN, SC

# MICROSTRUCTURAL EVOLUTION DURING A SOLID STATE TUBE PINCH WELD

Prepared for publication in the Proceedings of the ASME 2020 Pressure Vessel and Piping Conference, PVP2020, July 19-24, 2020, Minneapolis, Minnesota, USA, PVP2020-21308

**Paul S. Korinko**

March 2020

SRNL-STI-2020-00101

This work was prepared under an agreement with and funded by the U.S. Government. Neither the U.S. Government or its employees, nor any of its contractors, subcontractors or their employees, makes any express or implied:

1. warranty or assumes any legal liability for the accuracy, completeness, or for the use or results of such use of any information, product, or process disclosed; or
2. representation that such use or results of such use would not infringe privately owned rights; or
3. endorsement or recommendation of any specifically identified commercial product, process, or service.

Any views and opinions of authors expressed in this work do not necessarily state or reflect those of the United States Government, or its contractors, or subcontractors.

SRNL.DOE.GOV

## MICROSTRUCTURAL EVOLUTION DURING A SOLID STATE TUBE PINCH WELD

Paul S. Korinko

Savannah River National Laboratory, Aiken, SC USA

### ABSTRACT

*Microstructure development is examined for a specialized spot weld that is used as a solid-state closure process for stainless steel tubing, referred to as pinch welding. In order to elucidate the microstructural evolution of the weld, a series of test welds were made at nominal conditions using both tubes, used in test articles and production like components. These pinch welds normally terminate after twelve cycles of a 60 Hz AC weld process. In this study, tubes with different thermal processing history were welded from one to twelve cycles and the microstructure and weld variables after each individual weld cycle number were characterized using radiography and optical metallography. Two etchants were used that highlighted different microstructural features. The study revealed that: (1) this type pinch weld is largely complete after about six cycles of 60 Hz AC current, half the weld time utilized; (2) the resistance, deformation, and closure length approach “steady state” conditions after six cycles; and (3) both oxalic and nitric acid electrolytic etchants are useful for highlighting specific microstructural attributes of type 304L stainless steel. Finally, two distinct microstructural regions can be identified for these welds: the edge of the weld which is driven by concentrated deformation, recrystallization and grain growth and the center region which is more typical of forge welding and micro-asperity breakdown followed by diffusion and grain-growth. The bond line of annealed tubes exhibits fewer indications and less contamination than that of the partially annealed and as-received cold worked tubes.*

Keywords: Resistance Weld, Solid State, Stainless Steel

### NOMENCLATURE

A	Ampere
Hz	Hertz
PW	Pinch Weld
SS	Stainless Steel
CPW	Confined Pinch Weld

### 1. INTRODUCTION

Pinch welding is a unique application of a spot weld for closure of gas cylinder stems. This welding method is also known as tube closure welding and particularly suited for use in (potentially hazardous) gas storage cylinder (e.g. hydrogen), where particulate generation is to be avoided, and the application does not allow for typical tubulation through standard pressure fittings. Pinch welding uses bull nose electrodes with either 2.4 mm (3/32 inch) or 4.8mm (3/16 inch) radius electrodes. In one type of pinch welding, the tubes are confined from lateral spread during the weld with a die; i.e., it is a confined pinch weld. The final weld thickness is also limited by the thickness of the confining dies, 1.27 mm (0.050 inch). The confined weld is critical for applications where mating components have a 3.2 mm (0.125 inch) hole as a receptor. Unconfined welds that allows the tube to spread to diameters between 4.06 mm (0.16 inch) and 6.1 mm (0.24 inch) with thicknesses between 0.787 mm (0.031 inch) and 1.24 mm (0.049 inch). Unlike the traditional spot welds, the pinch welds are ideally solid-state welds [1-3]. The rationale for maintaining solid state welds is that the stems are used to seal hydrogen gas containers and solid-state welds reduce the amount of hydrogen that is absorbed in the weld metal. In addition, avoiding the melt, reduces the propensity to form weld expulsions and particulates that have an adverse effect on the component functionality.

A number of studies have been conducted at the Savannah River National Laboratory to better understand fabrication, damage, welding parameters and other influences on pinch welding. These engineering studies [4-12] show the effects of fill stem manufacturing practices on pinch weld quality. It was shown that machining oils can cause significant defects in the welds when the starting stock (forgings, tubing, bar stock, etc.) is not properly cut and smeared metal occurs which causes multiple interfaces that are not adequately cleaned or removed [4,5,6]. In an attempt to remove internal, loosely adherent particles or oxide films, rotary brushing was attempted. This treatment caused the spread of internal contamination and

promoted a lower quality weld than leaving low levels of contaminants [7]. Internal scratches are also of concern, so a detailed study showed that gouges as deep as 38  $\mu\text{m}$  (0.0015") can be welded over without adverse effects. Defects this deep are an order of magnitude greater than any defects found in the actual hardware [8].

The present method of pinch welding utilizes a weld controller essentially as a timer to start and stop the weld after 12 60 Hz cycles using 100% weld heat and a powerstat to adjust the primary voltage. Research was conducted to evaluate the weld controller's ability to control the weld using constant current where the waveform is chopped to maintain a constant current. These tests revealed that the process is sufficiently robust and the requirements readily achieved that the control mode was not detectable using the metrics selected. The effect of welding atmosphere, i.e., deuterium or air, indicated that there was little influence on the bond line appearance between the two atmospheres [9]. These corporate studies demonstrated that the pinch weld process is highly robust, yet occasionally unacceptable weld attributes are detected. Thus additional work to elucidate pinch weld quality attributes from the data was conducted. For instance, the weld inputs and outputs were characterized and modeled using a neural network that was able to correctly forecast weld bond line quality after proper training [10], in addition to process modeling [11]. Residual stresses of pinch welds have also been measured [12].

The deformation and recrystallization characteristics of pinch welds have been studied [13]. This study revealed that there is less grain growth across the grains than would be expected based on metallographic analysis. Based on the current description of pinch welding and the evolution of the bond line, one would expect a significant amount of diffusion across the bond interface, the referenced study indicated that grains did not grow across the interface as evidenced by the discontinuity in the crystallography of the grain across the interface.

In general, these studies provided engineering solutions to specific questions related to pinch welds. The evolution of the pinch weld and the microstructural events occurring during the weld were of interest though. Consequently, this study was envisioned and a systematic characterization of the weld microstructure as a function of weld cycles was conducted

## 2. MATERIALS AND METHODS

Pinch welds were made on forged Type 304L stainless steel (SS) stems with the geometry shown in Fig. 1. The stems met all the dimensional and chemistry requirements to be production components. The welds are made by inserting the stem into a weld fixture and tightening the confining anvils to 9.5 N-m (7 ft-lbs) of torque, a fill stem loaded into the weld fixture is shown in Figure 2. The hole in the front of the fixture is the location for the welding electrode to make mechanical and electrical contact with the stem.

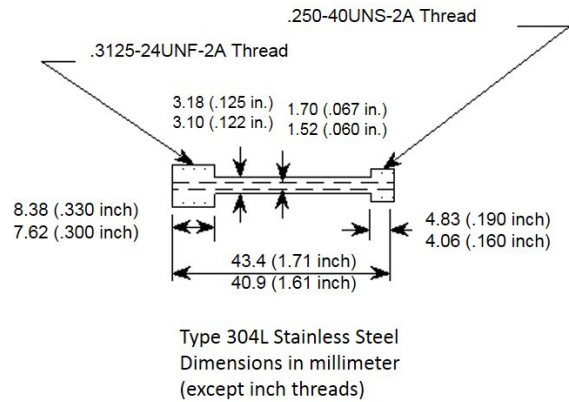


**FIGURE 1: GEOMETRY OF FILL STEMS USED IN THIS STUDY**

Pinch welds were made using the Savannah River National Laboratory (SRNL) pinch welder shown in Figure 3. This welder contains a prototypic production weld head and with a Heidenhain displacement gauge which is not present on the production welders. The weld head can apply forces up to approximately 7560N (1700 lbs.) and currents up to 5000A and operates on 60 Hz alternating current. The weld heat input is controlled by limiting the input voltage and monitoring the welding current, i.e., constant voltage mode, using a 440 V powerstat. The energy is calculated within the LabView control software and is presented with the post weld data metrics, as is the dynamic resistance, current, etc.

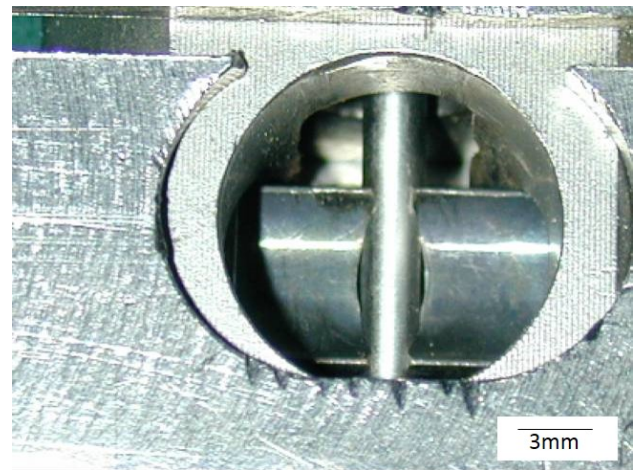


**FIGURE 2: STEM AND CONFINING DIES USED IN THIS STUDY**

The welds on the fill stems were made using standard fixtures with full restraint (the end of the stem was immovable along its axis) at the fill nubbin and partial restraint at the foot end; a single weld was made in each stem: the same conditions that are used for production products. The welds on tubing were made using a special tubing fixture that provides full restraint at both ends of the weld. Pinch welds on tubing were made at 19

mm ( $\frac{3}{4}$ " ) intervals with up to eight welds on each tube. The confined pinch welds were made using constant voltage control for all number of cycles of 60 Hz AC current between 1 and 12 to observe how the pinch weld microstructure evolves with time/number of weld cycles. In this control mode, the primary voltage from the powerstat is reduced to the target voltage and the secondary current is directly related to the input. This method of controlling the current has been used extensively. The welds are completed by applying the force to the electrode which crushes the tube, the current is then applied and the interfaces interact to form the weld. Since AC current is used, the tube actually cycles from red heat to cold at 60Hz.

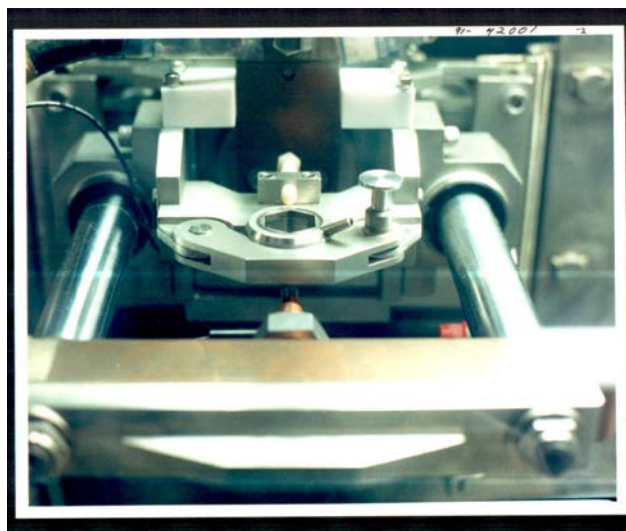


**FIGURE 3: WELDER USED IN THIS STUDY.**

The electrodes are wrought copper with tungsten tips brazed in place and machined to a 4.8 mm ( $\frac{3}{16}$  inch) bull nose. An electrode force of 5560 N (1,250 lbs.) was selected to weld the samples at a target current of 3850 amperes for both the tubing and the stems. Due to a change in weld systems, the stems and tubes were welded at different weld voltages but at nominally the same weld current. Stems were welded at 415 V compared to the tubes which were welded at 369 V. To prevent or at least minimize oxidation of the interfaces during welding, nitrogen gas was passed through the stems during processing; tubes were welded in a static atmosphere of 203 kPa (30 psia) nitrogen. This environment has been shown to protect the welds from oxidation and provide a similar welding environment to hydrogen within tubes [9].

The thickness of the welds was measured using a point micrometer, and the closure length was determined using digital radiography. The radiographs were inspected for material extrusion at the end of the welds or expulsion. Metallographic samples were prepared transverse to the tube axis near the center of the weld, mounted in epoxy, ground, and polished using standard metallographic sample preparation techniques for cross-sectional microscopic examination. The metallographic

samples were prepared by grinding from 240 to 600 grit silicon carbide paper and polished to 1  $\mu$ m diamond and then electrolytically etching with 10% oxalic acid at a current density of 0.2 mA/cm<sup>2</sup> for 15 to 90s. The stems were examined with an optical microscope at magnifications from 50 to 500 times. After initial microscopy, all the stem samples were re-polished and electrolytically etched with 30% nitric acid at 1.2V and reexamined. The nitric acid etching required multiple iterations of etching and polishing with one  $\mu$ m diamond slurry to reveal a scratch free microstructure. All the tubing samples were examined using optical microscopy in the transverse orientation after electrolytically etching with oxalic acid; these samples were imaged using differential interference contrast. Selected tubing samples were re-polished, electrolytically etched with nitric acid, and examined optically to reveal other microstructural features, similarly to the stems.

### 3. RESULTS AND DISCUSSION

The starting microstructure for the fill stem is shown in Figure 4 after etching with two different acids. The as-received stems have equiaxed grains, with some annealing twins evident. The stems did not exhibit deformation twins. The stems have a specification requirement of a grain size of ASTM of five or finer and a Rockwell A hardness of 47-58 HRA.

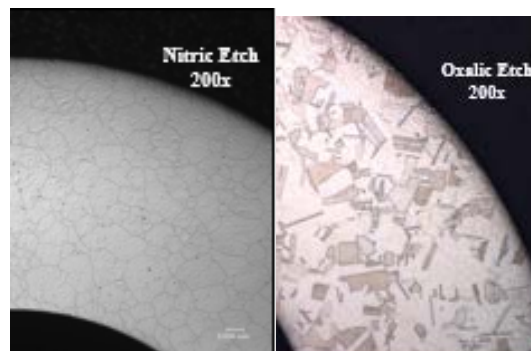


**FIGURE 4: INITIAL MICROSTRUCTURE OF A FILL STEM ETCHED WITH A) NITRIC ACID AND B) OXALIC ACID**

The weld data, set point and output, for the stems are presented in Tables 2 and in Fig. 5. The current is less than the target for the first several cycles. This partly results from the controller operation and the calculation of the reported RMS current. For example, the peak current for the first cycle is about 3804 A compared to the target of 3850 A. The RMS current is calculated by the data acquisition system (DAS) to be 2573 A compared to 2690 A determined by simply dividing the peak current by the square root of two. Statistical analysis of pinch weld data currents at nominally 3750 A exhibit a standard deviation of 4.4 A.



### 3.1 Dimensional Results

**TABLE 1: WELD CONDITIONS AND RESULTS FROM THE DATA ACQUISITION**

Serial No.	Cycles	Voltage (V)	Force (N)	RMS Current (A)	Dyn. Res. (mΩ)	Energy (J)	RMS Volts	Net Displ. (mm)
20641	1	415.2	5587	2574	0.238	12.7	0.612	0.076
20451	2	414.7	5593	3352	0.247	87.2	0.828	0.203
X0130	3	415.1	5590	3501	0.250	130.4	0.875	0.305
20539	4	414.9	5594	3589	0.243	184.8	0.871	0.330
20477	5	415.4	5577	3649	0.239	240.1	0.871	0.336
20502	6	415.4	5591	3684	0.229	301.0	0.844	0.406
X0100	7	414.6	5586	3705	0.227	339.5	0.841	0.432
X0107	8	414.8	5587	3722	0.222	386.3	0.827	0.457
20469	9	415.1	5579	3741	0.220	434.8	0.824	0.508
X0120	10	415.0	5582	3756	0.214	475.8	0.805	0.508
X0127	11	415.7	5584	3771	0.213	526.2	0.804	0.559
X0101	12	413.7	5590	3762	0.210	565.5	0.791	0.533
X0126	13	NA	NA	3794	0.211	583.2	0.801	0.559
X0117	14	413.8	5589	3804	0.206	663.0	0.784	0.559

The thickness and closure length results for the stems are listed in Table 4. As expected, the thickness decreases with increasing number of cycles and the closure length increases with increasing cycles. In a complementary study, it was shown that the thickness at zero cycles depends on the material hardness, but the final weld thickness stabilizes at about 1.19 mm (0.047 inch), regardless of initial hardness. The final thickness is limited by the presence of the Hastelloy X confining dies, and the extent of “ear” formation, material extruded around the confining dies due to deformation of the tube. In the case of fully completed welds, the confining dies act like a positive stop for the stem collapse so this dimension is limited by the equipment geometry.

The X-ray closure measurements indicate no closure occurs for the first several cycles, which is consistent with the metallurgical results discussed below and observations during welding in flowing gas. The radiographic closure lengths were determined from face and side view radiographs.

### 3.2 Metallography Results

Metallographic samples were prepared and examined for every test weld. Samples were electrolytically etched with oxalic acid and examined, then re-prepared and electrolytically etched with nitric acid and examined. These etchants bring out different features as can be seen in Figure 7 for the stem sample after 3 cycles. The oxalic acid etched sample indicates that fine grains may be present but does not show them as clearly as the nitric acid etch. Oxalic etching reveals clear evidence of deformation twinning in the bulk away from the weld interface, as well as plastic deformation bands. On the other hand, the nitric acid etch shows numerous fine grains at the interface and in the heavy deformation zone at the tube wall and primary crush zone, also called the “crow’s foot”, while there is little evidence of either flow lines or deformation twins. Thus, the use of both etchants provides complementary information to characterize the metallurgical structure of these welds as each display different metallurgical / microstructural attributes.

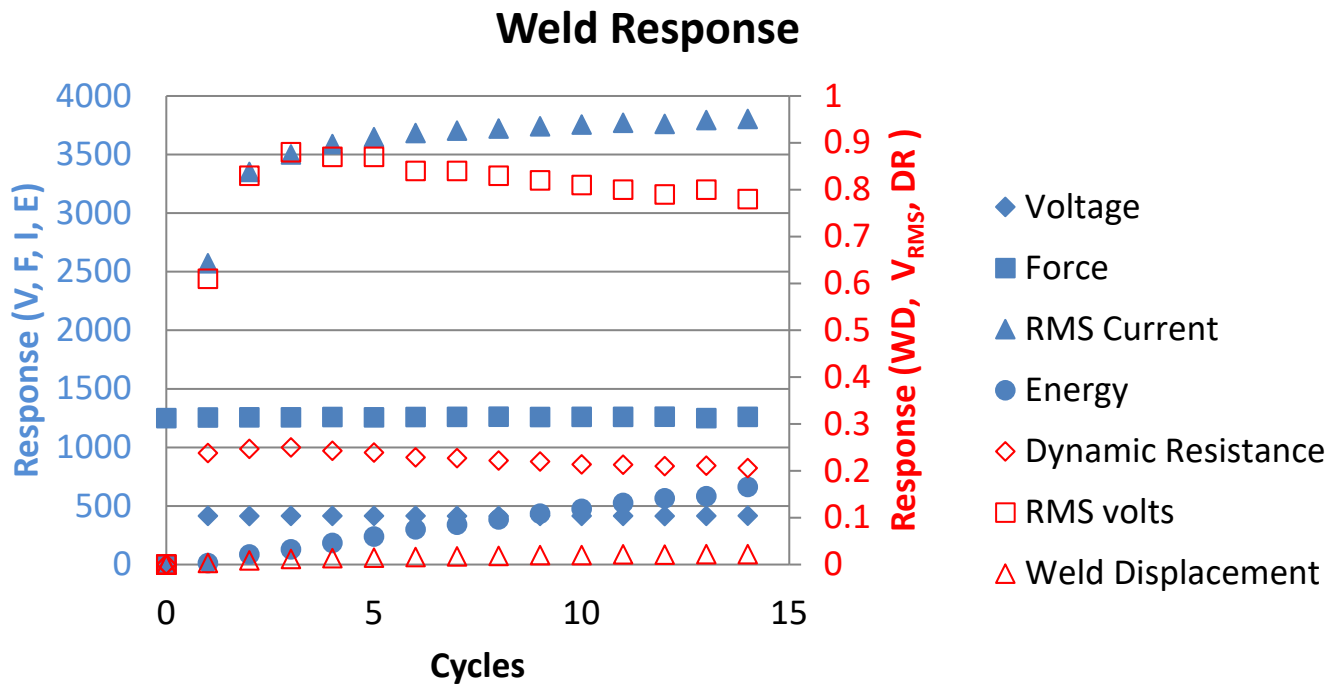


**FIGURE 5: PLOT OF WELD CONDITIONS, DATA FROM TABLE 1.**

**TABLE 2: DIMENSIONAL MEASUREMENTS OF STEMS AFTER WELDING FROM 0 TO 14 CYCLES.**

N	Weld ID (stem)	Thick (mm)	C L. (mm)	Weld ID Tube	Thick (mm)	CL (mm)	Weld ID Tube	Thick (mm)	CL (mm)	Weld ID Tube	Thick (mm)	CL (mm)
0	X0106	NA	0.000	AR0	1.956		PA0	1.905	0.000	FA0	1.753	0.000
1	20461	2.032	0.000	AR1	1.778	0.000	PA1	1.702	0.000	FA1	1.575	0.000
2	20451	1.905	0.000	AR2	1.575	0.000	PA2	1.549	0.000	FA2	1.397	0.991
3	X0130	1.778	0.000	AR3	1.473	0.000	PA3	1.473	0.686	FA3	1.372	1.143
4	20539	1.651	1.168	AR4	1.422	1.270	PA4	1.372	1.321	FA4	1.321	1.854
5	20477	1.524	1.702	AR5	1.397	1.575	PA5	1.321	1.854	FA5	1.295	2.083
6	20502	1.473	2.540	AR6	1.346	2.286	PA6	1.321	2.286	FA6	1.270	2.413
7	X0100	1.448	3.124	AR7	1.321	2.896	PA7	1.295	2.591	FA7	1.245	2.870
8	X0107	1.422	3.556	AR8	1.270	3.226	PA8	1.295	2.896	FA8	1.219	3.073
9	20469	1.422	3.937	NA	NA	NA	NA	NA	NA	NA	NA	NA
10	X0120	1.397	3.988	AR10	1.219	3.429	PA10	1.245	3.454	FA10	1.194	3.404
11	X0127	1.346	4.191	NA	NA	NA	NA	NA	NA	NA	NA	NA
12	X0101	1.321	4.267	AR12	1.219	3.835	PA12	1.194	3.759	FA12	1.194	3.556
13	X0126	1.295	4.318	NA	NA	NA	NA	NA	NA	NA	NA	NA
14	X0117	1.270	4.470	AR14	1.168	4.115	PA14	1.168	3.454	FA14	NA	4.039

N is number of weld cycles @60 Hz, Thick is post weld thickness, and CL is closure length measured radiographically, AR## As received tubing sample, FA## Fully anneal tubing sample (1149C/2 hours), PA## Partially anneal tubing sample (927C/20 minutes).

Typical Standard Deviations for the measurements, based on four welds made at 3415 A, 12 cycles, 339 V, are as follows (6):

Thickness: 53  $\mu$ m

Closure Length: 21  $\mu$ m

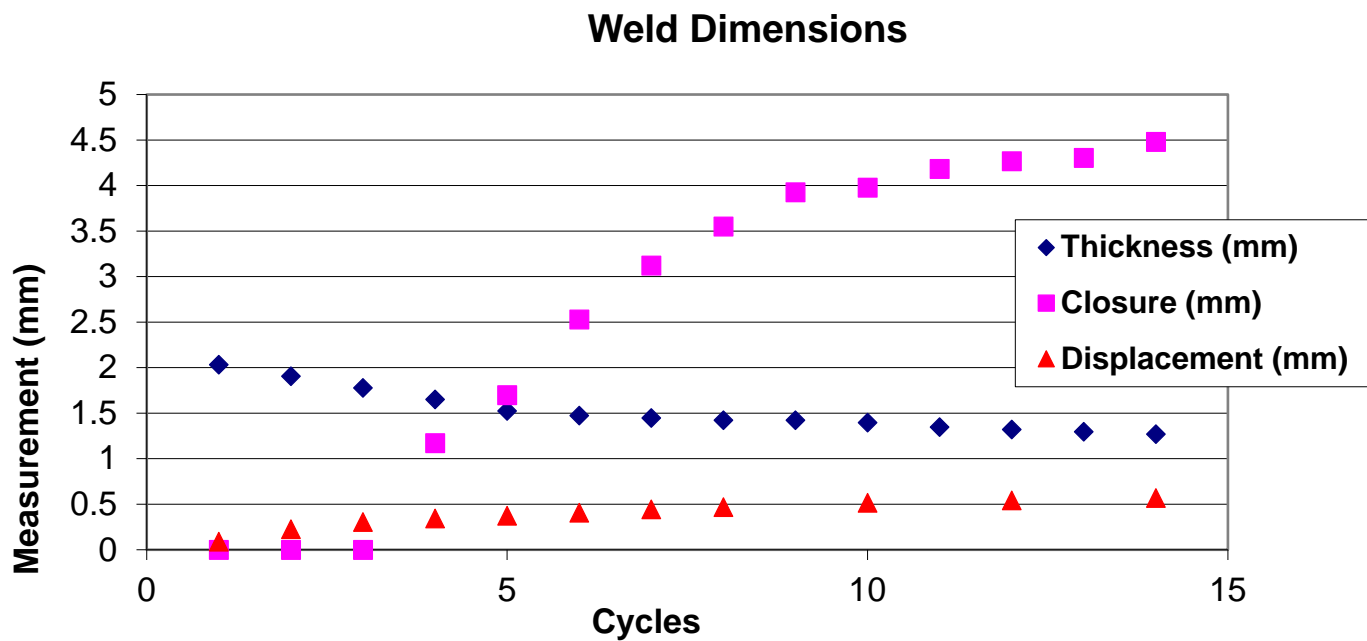


**FIGURE 6: DIMENSIONAL MEASUREMENTS OF STEMS AFTER WELDING FROM 0 TO 14 CYCLES, DATA FROM TABLE 2.**

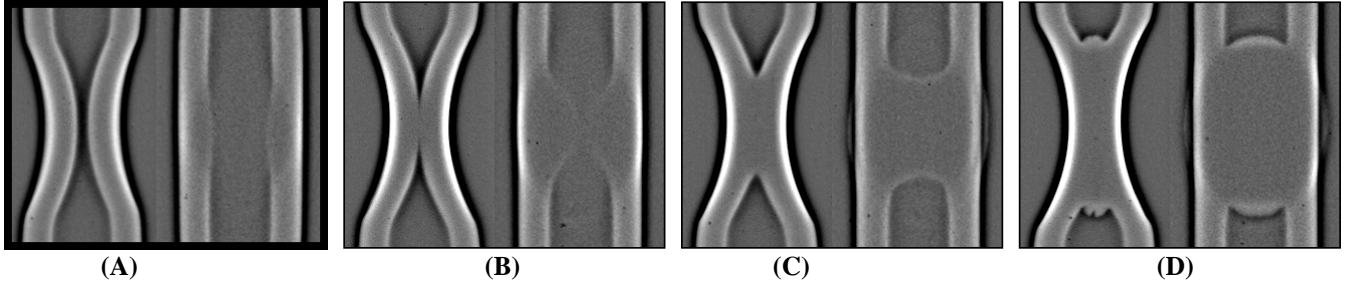


**FIGURE 7:** X-RAY IMAGES OF WELDS IN THE EDGE AND PLAN VIEW SHOWING CLOSURE LENGTH AFTER A) 1 CYCLE, B) 4 CYCLES, C) 6 CYCLES AND D) 12 CYCLES

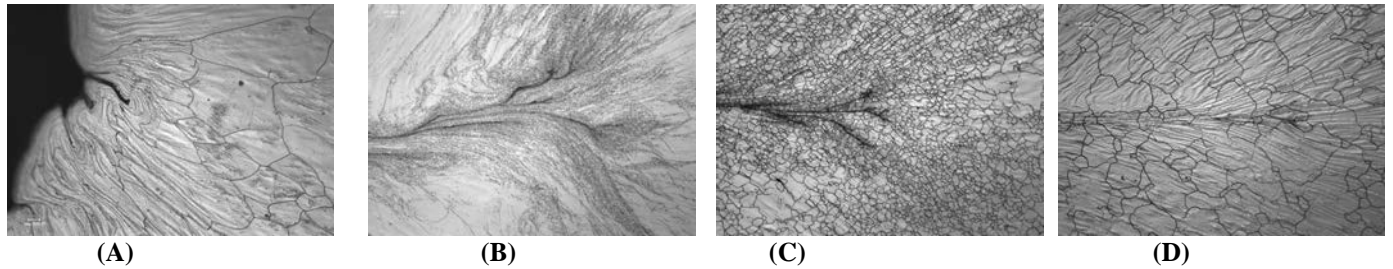


**FIGURE 8:** MICROSTRUCTURAL EVOLUTION OF THE CROW'S FOOT OF THE PINCH WELD AFTER A) 0, B) 3, C) 6, AND D) 12 CYCLES

were determined using different magnifications at differing locations across the weld interface. In particular, the extent of recrystallization was clearly revealed from the 500X magnification images of “crow’s foot” of the stem welds. The term crow’s foot refers to the end of the weld where the tube is initially crushed; this term is used since it often resembles a crow’s foot with several dark etch lines or folds. Other characteristics, such as the grain size, flow lines, and the presence of recrystallized grains required higher or lower magnifications to reveal the desired details. Some photomicrographs were taken at 1000X in order to resolve the very fine grains present in the samples welded at up to four cycles. The grain size was measured in the crow’s foot, (Fig.8), while in the width of the heat affected zone (HAZ), the area in the center of the weld that exhibits microstructure changes, was at the weld center and includes the entire weld width (Fig. 9).

The weld evolution can be described with cold work crushing the tube and the presence of deformation and twinning in the crow’s foot. At the first cycle, the grains in the crow’s foot become elongated but the faying surfaces are not in contact. At second cycle, etch pits are visible along the high deformation zone. It is not clear if the etch pits are due to dislocation alignment or the onset of recrystallization. The tube faying surfaces are still not in contact. Recrystallization occurs at the third cycle and the tube collapses and nearly makes contact along the entire surface. At the fourth cycle, the onset of grain growth occurs and consistent with the X-ray results, there is bonding across the entire faying surface. Grain growth continues until about cycle 8 and then there is a stabilization of the grain size. Several welds after a few cycles that exhibit the changes in the microstructure are shown in Figure 8 for the crow’s foot and the at the center of the weld in Figure 9.

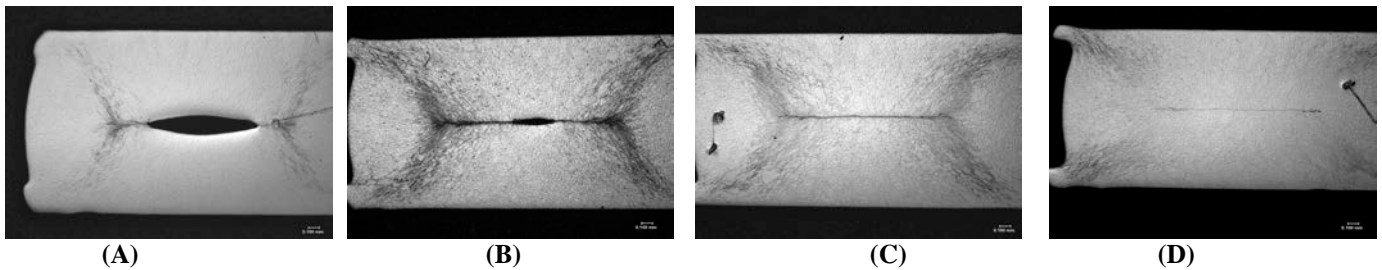


**FIGURE 9:** OBSERVATION OF THE CLOSURE AT THE CENTER OF THE PINCH WELD AFTER A) 3, B) 4, C) 5 AND D) 7 CYCLES.



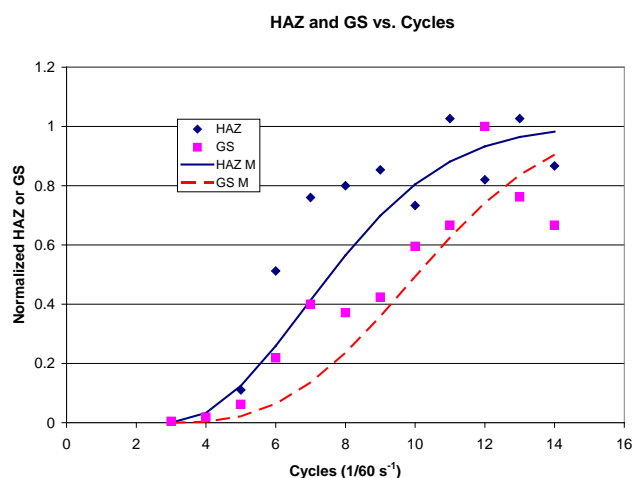


**FIGURE 10: HEAT AFFECTED ZONE AND GRAIN SIZE MODEL BASED ON THE AVRAMI EQUATION.**

The grain size and HAZ width were determined from the nitric acid etched samples. It is postulated that these data and attributes could be modeled using common thermal process phenomenology for nucleation and growth, such as the generalized Avrami equation [14]. The grain size and HAZ data for the stem samples are shown graphically in Figure 10. These data show a non-linear response with number of cycles. They also show a delay, perhaps an incubation period, before there are changes in the response. There is also a tapering off of the grain size and HAZ width. These are likely associated with the total heat input of the weld.

### 3.3 Weld Parameter Results

The primary method of demonstrating acceptable welding in production is to verify that the weld parameters-RMS voltage, electrode force and number of cycles, are within acceptable limits. The limits of each parameter are determined by test welds. One calculated quantity that may provide additional information about weld quality is the so-called “dynamic” resistance. This quantity is calculated by dividing the peak voltage by the peak current during each cycle. A plot of the “dynamic” resistance for stems and some heat treated tubes as a function of cycles is shown in Figure 11. The dynamic resistance increases from cycle 1 to cycle 2, and then monotonically decreases during subsequent cycles, finally becoming approximately constant at about ten cycles. These results are consistent with a twelve cycle weld that is continuous. Similar to the dynamic resistance, the weld voltage measured across the electrodes peaks at the first cycle and gradually decreases with subsequent cycle. There is a slight shift in the time at which the peak current and peak voltage are detected, but the difference was on the order of one or two tenths of a millisecond. This offset in the time of the voltage and current maxima is an indication of capacitive and inductive components of the system electrical impedance.

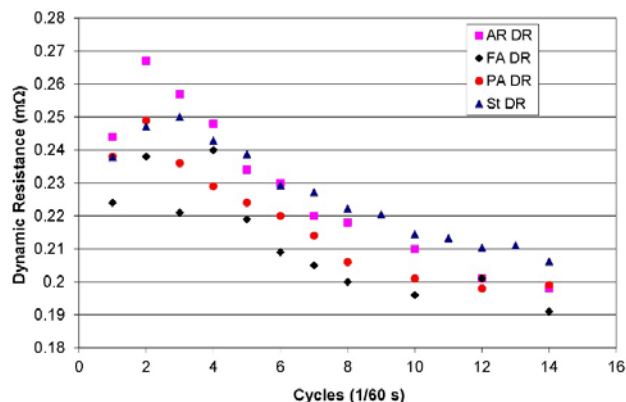


**FIGURE 11: THE DYNAMIC RESISTANCE DECREASES WITH INCREASING CYCLES AFTER CYCLE 2**

The starting and evolutionary dynamic resistance is consistent with the starting microstructure and heat treatment. The fully annealed (FA) samples have the lowest resistance, as would be expected, and the as-received (AR) tubing samples and stems have the highest, which is consistent with being in the annealed condition with large grains and cold worked states, respectively. In addition to these influences, additional deformation transformation mechanisms such as deformation induced martensite and deformation twinning may promote the differences in the resistance. A statistical analysis of the data indicates that the mean value of the AR and stem dynamic resistance has a 90% chance of being from a different population than the fully annealed, while there is little evidence to suggest that the PA samples are from different populations.

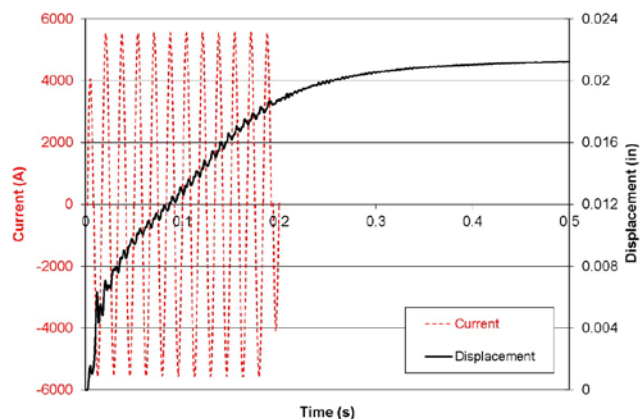


**FIGURE 12: TYPICAL DISPLACEMENT CURVE AND CURRENT DATA FOR A 12 CYCLE WELD SHOWING THE ELECTRODE MOVEMENT DURING AND AFTER THE WELD.**

The electrode displacement and weld current data are plotted in Figure 12. The deformation during the first cycle is approximately 30% of the total deformation that occurs. A

significant amount of thermal softening occurs during this cycle. It is apparent that more than 70% of the total displacement occurs during the first six weld cycles with the remaining 30% occurring after the seventh cycle. The electrode displacement is also loosely correlated with the closure length increasing in during the latter cycles, based on closure data provided in Table 4. It is interesting to note that the electrodes continue to indicate movement after the heat source is shut off. This continued movement may be due to conduction of the heat away from the weld interface and into the surrounding metal which promotes additional deformation of the tube axially to increase the bond length or simply due to thermal contraction of the weld.

#### 4. DISCUSSION

The weld microstructure evolves differently in the “crow’s foot” (weld edges, Fig. 8) compared to the center of the pinch weld (Fig. 9). The crow’s foot is driven by plastic strain from the shearing and collapse of the tube, recrystallization due to extensive localized deformation and heating, followed by grain growth. The center section of the weld is similar to forge welding with normal forces and interfacial heating. The temperature of the weldment increases as current is passed around and through the collapsed area. The force is applied and then the current, which heats the tube and brings the faying surfaces into intimate contact and promotes oxide breakdown, recrystallization and grain growth.

At the crow’s feet, there is a high degree of plastic flow including extrusion of the side wall surfaces into the bond interface (Fig. 8). This area heats first and also has the highest plastic strain due to the constraint. This complex deformation creates new fresh surfaces and assists in disrupting and damaging the existing metal surface oxides and contamination. These intimately contacting and freshly cleaned surfaces are able to form a diffusional bond. The extensive and rapid recrystallization initiated in the crow’s foot and beyond, promotes microstructural homogeneity across the interface.

In the center of the weld, the confining dies and process geometry limit the extent of deformation in the transverse direction and the way the tube is fixtured in the welder limits the axial expansion to about 0.38 mm (0.015”). Hence, surface disruption in this area occurs primarily on a micro-asperity scale, and the break-up of surface oxides and contamination is less than at the edge areas. The Joule heating may be more intense in this area due to interfacial heating. Fusion welds and expulsion defects are observed near the center of the weld. These defects are often generated at lower forces and high current (i.e., hot welds). Recrystallization will homogenize the microstructure across the bond interface, provided the interfacial grain boundaries are not pinned by inclusions. (Inclusions are quite stable in stainless steels, and are not solutionized in pinch welds). It appears that the bonding in the center area of the weld is initially poor and progresses to a diffusional bond as the number of cycles increases. The bond evolves to a situation much like the conditions described in the acceptance criteria, from a

distinct bond line with no recrystallization and grain growth to an obscured or completely consumed bond line with extensive recrystallization and grain growth with little or no evidence of a prior interface. However, for solid state bonds with no incipient melting, like those prepared for this study, the center of the weld is formed with less deformation and is potentially of slightly lower quality than the edges.

#### 4. CONCLUSION

The evolution of microstructure changes with time occurs by two mechanisms for solid state pinch welds. The edges or crow’s feet are driven by mechanical and thermal processes while the center is controlled primarily by Joule heating.

Extensive deformation promotes recrystallization between one and three heat cycles. The pinch weld deformation is approximately 80% complete after six cycles. The major recrystallization and grain growth events are completed after eight cycles. The grain size continues to increase but at a much lower rate.

The cycle to cycle resistance as determined by peak V divided by Peak I is reduced through about six cycles at which point it reaches a plateau. This lack of change is consistent with the relative stasis that is observed in the microstructure.

Nitric and oxalic acid etchants are complementary and reveal different features of pinch weld microstructures.

#### ACKNOWLEDGEMENTS

The authors would like to acknowledge the contributions and technical input from B. West of Savannah River Tritium Enterprise and the recognize the contributions of the Materials Test Facility (MTF) technicians and Carol Kestin for conducting and interpreting the metallography, the Materials Technology Section metallographer (Tony Curtis) and assistants for additional metallography and J. Levings for funding the Project NORMAN task as part of the Technology Investment Program. We would also like to recognize the contributions of Daniel Hartman, Vivek Dave, Mark Cola, and Bill King for critical reviews and insightful comments. This document and the research were prepared and conducted for the U.S. Department of Energy under contract number DE-AC09-08SR22470 with Savannah River Nuclear Solutions.

#### REFERENCES

1. Kianersi, Danial, Mostafaei, Amir, Amadeh, Ahmad Ali, “Resistance spot welding joints of AISI 316L austenitic stainless steel sheets: Phase transformations, mechanical properties and microstructure characterizations,” *Materials and Design* 61 (2014) 251–263
2. Karcı, Feramuz, Kac, Ramazan, Gündüz, Süleyman, “The effect of process parameter on the properties of spot welded cold deformed AISI304 grade austenitic stainless steel,” *Journal of Materials Processing Technology* 209 (2009) 4011–4019.

3. Moshayedi, Hessamoddin, & Sattari-Far, Iradj  
“Numerical and experimental study of nugget size growth in resistance spot welding of austenitic stainless steels,” *Journal of Materials Processing Technology* 212 (2012) 347– 354.
4. Korinko, P.S. & Arnold, K.F., Optimization Study for Fill Stem Manufacturing and Pinch Weld Processing, SRNL Report, September 2006
5. Korinko, P. S., and Maxwell, D N., Fill Stem Manufacturing Changes and Pinch Weld Qualifications, SRNL Report, Feb 21, 2008
6. Korinko, P. S., and Maxwell, D N., Pinch Weld Testing to Support Change in Manufacturing Oil at the KCP, SRNL Report,, Feb 21, 2008
7. Korinko, P.S., Effect of Brushing on Pinch Weld Quality, SRNL Report, September 2005. (12-15-05)
8. Korinko, P.S., Effect of Scratches on Pinch Weld Quality, SRNL Report, September 2005. (11-10-05)
9. Korinko, P.S. & Howard, S. R., Effect of Constant Current on Pinch Welds, SRNL Report, September 2005.
10. Korinko, P.S. & Howard, S. R., Fisher, G. H., , Evaluation of a New Pinch Resistance Test Method, SRNL Report, September 2005.
11. Korinko, P.S., Effect of Atmosphere on Pinch Weld Quality, SRNL Report, Sept. 2005
12. Bowers, J.A., and Korinko, P.S., Exploration of Summary Data Sheets of Pinch Weld Experiments and Draft Neural Network Models Forecasting Weld Closure Length (U), SRNL Report, October 2003.
13. Hartman, D.A., Korinko, P.S., Tolk, N.R., Malene, S.H., Smith, M.G., Cola, M.J., Dave’, V.R., Miller, J.P., & King, W. H., In-Process Monitoring of Pinch Welding: An Investigation into a Bond Quality Metric, 7th International Conference on Trends in Welding Research, May 16-20, 2005 - Pine Mountain, Georgia, USA
14. Korinko, P.S., Pechersky, M.J., Zeha, D.L., McKinney, G.J., Reister, L, Blau, P., Lara-Curzio, E., “Characterization of Confined Pinch Welds in Type 304L Stainless Steel”, 6th International Conference on Trends in Welding Research, 15-19, April 2002, Callaway Gardens Resort, Pine Mountain, Georgia USA", ASM International
15. Necker, C. T., Marchi, A.N., Smith, M.G., Multi-cycle Pinch Welding of 304L Tubes: Inhomogenities in Deformation and Recrystallization Textures and Microstructures”, ICOTOM 15, June 1- 6, 2008, Pittsburgh, PA.
16. Porter, D.A. and Easterling, K.E., Phase Transformations in Metals and Alloys, Van Nostrand Reinhold, UK, 1981.